Supporting Information

Eu-MOF and its composites as turn-off fluorescence sensors for p-nitrophenol with the application in monitoring catalytic reduction reaction

Bing-Bing Xing,[a] Yue-Shu Wang,[a] Tao Zhang,[a] Jing-Yi Liu,[a] Huang Jiao,[a] and Ling Xu*[a]

[a.] *Key Laboratory of Macromolecular Science of Shaanxi Province, School of Chemistry & Chemical Engineering, Shaanxi Normal University, Xi'an 710062, Shaanxi Province, P. R. China*

Table S1. Crystal data and structure refinement for Eu-MOF.

Empirical formula	$C_{24}H_{19}N_7O_{14}Eu_2$
Formula weight	933.38
Crystal system	triclinic
Space group	P-1
a/Å	8.1327(3)
b/Å	13.4199(14)
c/Å	16.4494(5)
α/°	76.483(5)
β/°	88.538(3)
γ/°	84.360(5)
Volume/Å^3	1737.1(2)
Z	2
ρ_{calc}g/cm^3	1.784
μ/mm^{-1}	26.209
F(000)	900.0
Crystal size/mm^3	0.20 × 0.12 × 0.10
2θ range for data collection/°	5.526 to 178.922
Reflections collected	26180
Independent reflections	7179 [R_{int}= 0.0870, R_{sigma}= 0.0592]
Data/restraints/parameters	7179/36/424
Goodness-of-fit on F^2	1.059
Final R indexes [I≥2σ(I)]	R_1= 0.1038, wR_2= 0.2772
Final R indexes [all data]	R_1= 0.1209, wR_2= 0.2917

$R_1 = (\Sigma||F_o| - |F_c|| / \Sigma |F_o|)$. $wR_2 = [\Sigma (w(F_o^2 - F_c^2)^2) / \Sigma (w |F_o^2|^2)]^{1/2}$

Table S2. Selected bond distances (Å) and bond angles (º) of Eu-MOF.

Bond distances (Å)	
Eu1-O1=2.325(10)	Eu2-O1^4=2.407(10)
Eu1-O12=2.341(9)	Eu2-O11=2.349(9)
Eu1-O13^2=2.368(11)	Eu2-O14^5=2.322(11)
Eu1-O22=2.426(11)	Eu2-O21=2.432(13)

Eu1-O24^{3}=2.368(9)	Eu2-O23^{6}=2.339(9)
Eu1-O31=2.389(9)	Eu2-O31=2.565(10)
Eu1-O1W=2.356(14)	Eu2-O32=2.509(11)
	Eu2-O2W=2.513(17)
Bond angles (º)	
O1-Eu1-O12=131.6(4)	O11-Eu2-O21=116.8(4)
O1-Eu1-O13^{2}=78.6(4)	O11-Eu2-O22=72.2(4)
O1-Eu1-O22=145.4(4)	O11-Eu2-O31=76.0(4)
O1-Eu1-O24^{3}=75.4(4)	O11-Eu2-O32=126.9(4)
O1-Eu1-O31=114.9(4)	O11-Eu2-O2W=82.1(5)
O1-Eu1-O1W=75.5(5)	O14^{5}-Eu2-O1^{4}=74.8(4)
O12-Eu1-O13^{2}=79.9(4)	O14^{5}-Eu2-O11=80.4(4)
O12-Eu1-O22=75.4(4)	O14^{5}-Eu2-O21=78.3(4)
O12-Eu1-O24^{3}=151.8(4)	O14^{5}-Eu2-O22=83.0(4)
O12-Eu1-O31=96.0(4)	O14^{5}-Eu2-O23^{6}=81.1(4)
O12-Eu1-O1W=74.5(5)	O14^{5}-Eu2-O31=143.6(4)
O13^{2}-Eu1-O22=87.6(5)	O14^{5}-Eu2-O32=148.1(4)
O13^{2}-Eu1-O31=163.5(4)	O14^{5}-Eu2-O2W=134.0(5)
O24^{3}-Eu1-O13^{2}=101.8(4)	O21-Eu2-O22=46.7(3)
O24^{3}-Eu1-O22=76.6(4)	O21-Eu2-O31=88.1(4)
O24^{3}-Eu1-O31=74.3(4)	O21-Eu2-O32=74.3(4)
O31-Eu1-O22=75.9(4)	O21-Eu2-O2W=146.7(5)
O1W-Eu1-O13^{2}=113.9(6)	O23^{6}-Eu2-O1^{4}=78.4(3)
O1W-Eu1-O22=138.7(5)	O23^{6}-Eu2-O11=154.0(4)
O1W-Eu1-O24^{3}=127.6(5)	O23^{6}-Eu2-O21=76.7(4)
O1W-Eu1-O31=79.9(5)	O23^{6}-Eu2-O22=123.2(4)
O1^{4}-Eu2-O21=145.7(4)	O23^{6}-Eu2-O31=128.6(3)
O1^{4}-Eu2-O22=146.3(3)	O23^{6}-Eu2-O32=76.9(3)
O1^{4}-Eu2-O31=126.0(4)	O23^{6}-Eu2-O2W=98.1(5)
O1^{4}-Eu2-O32=122.0(4)	O31-Eu2-O22=63.7(3)
O1^{4}-Eu2-O2W=60.3(5)	O32-Eu2-O22=90.0(3)
O11-Eu2-O1^{4}=79.3(4)	O32-Eu2-O31=51.7(3)

Symmetry codes: ^{1}.-1+*x*, *y*, *z*; ^{2} 1-*x*, 1-*y*, 1-*z*; ^{3} 1-*x*, 1-*y*, -*z*; ^{4} 1+*x*, *y*, *z*; ^{5} 2-*x*, 1-*y*,1-*z*; ^{6} 2-*x*, 1-*y*, -*z*.

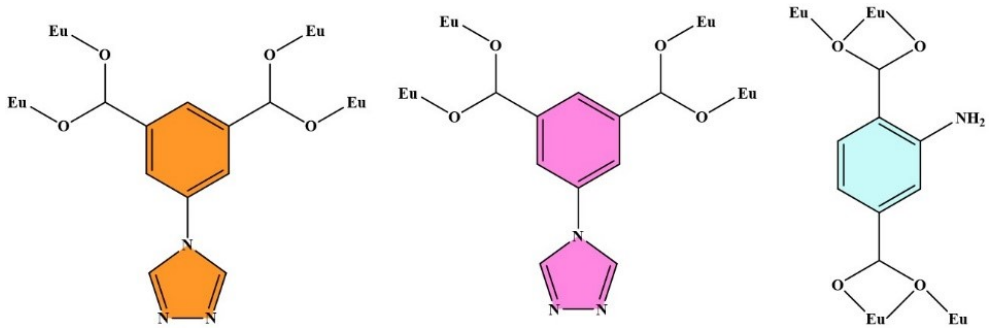

Figure S1. The coordination modes of TIPA^{2-} and NBDC^{2-} ligands in Eu-MOF.

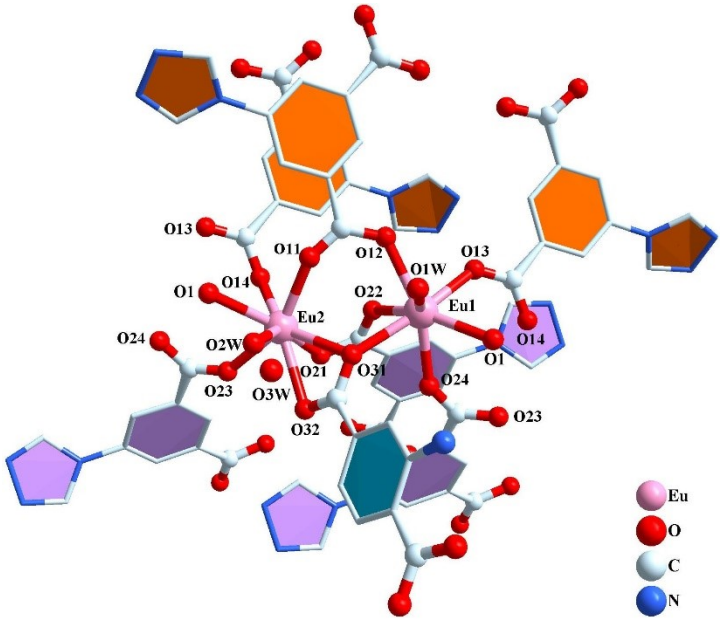

Figure S2. The coordination spheres of Eu1 and Eu2 in Eu-MOF.

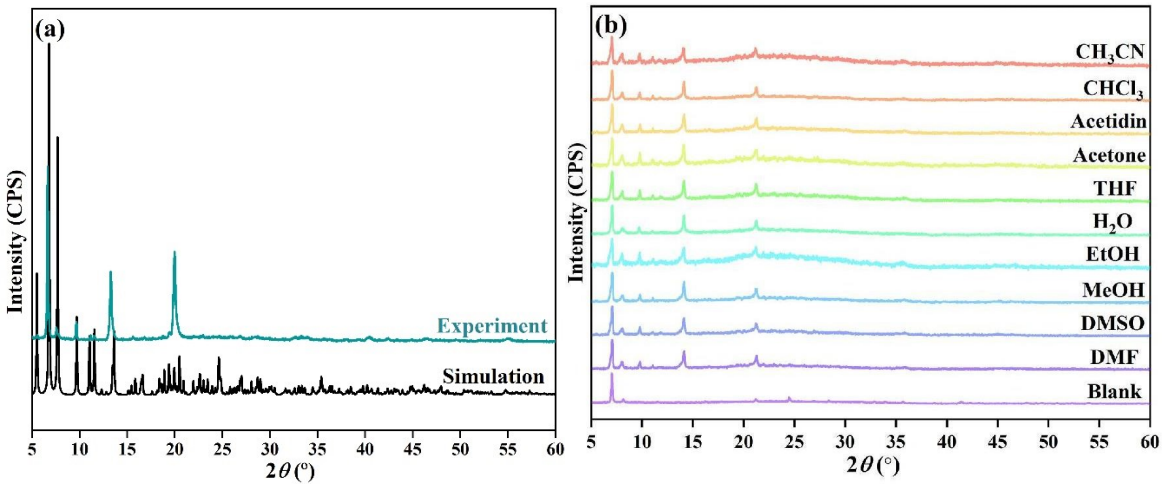

Figure S3. (a) The experimental PXRD pattern of the Eu-MOF bulk sample compared to the simulated one from the single crystal data; (b) PXRD patterns of Eu-MOF immersing in water and nine kinds of organic solvents for 5 h.

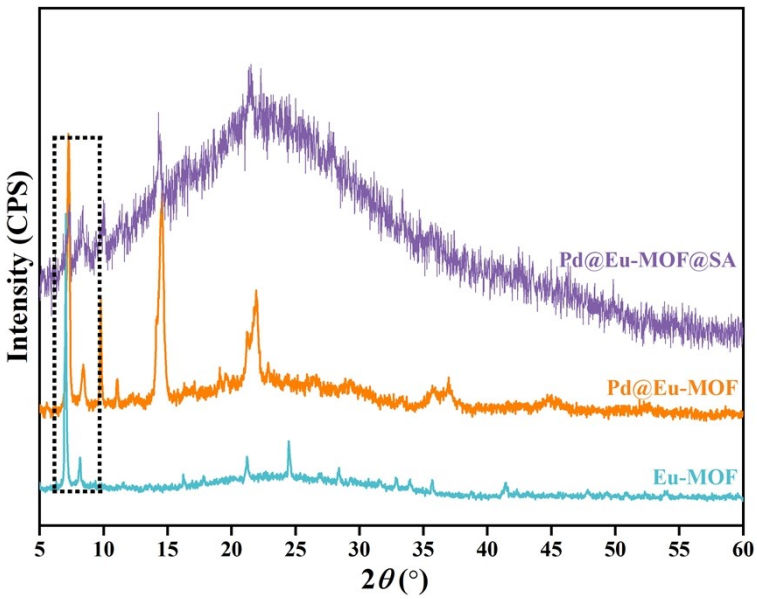

Figure S4. PXRD patterns of Eu-MOF, Pd@Eu-MOF, and Pd@Eu-MOF@SA.

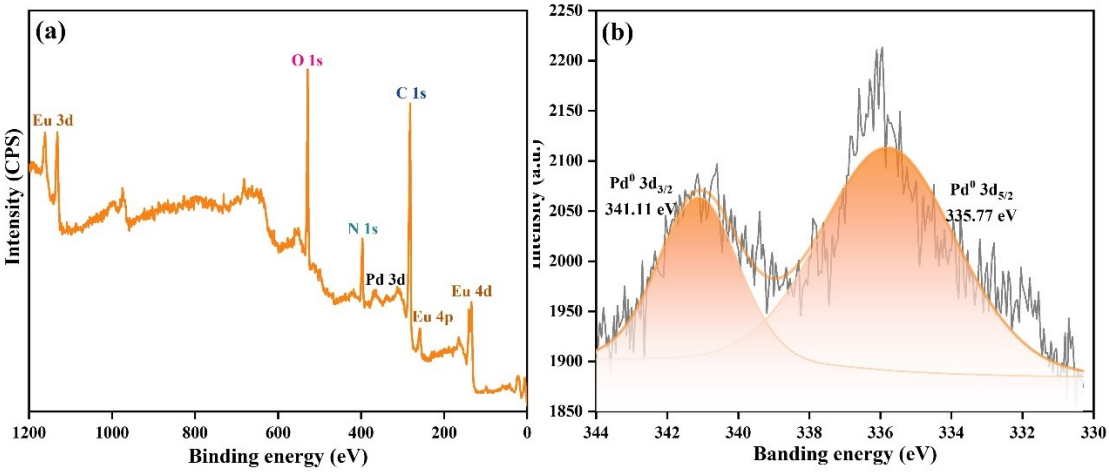

Figure S5. The XPS spectra of Pd@Eu-MOF (a) and Pd^0 3d (b) in Pd@Eu-MOF.

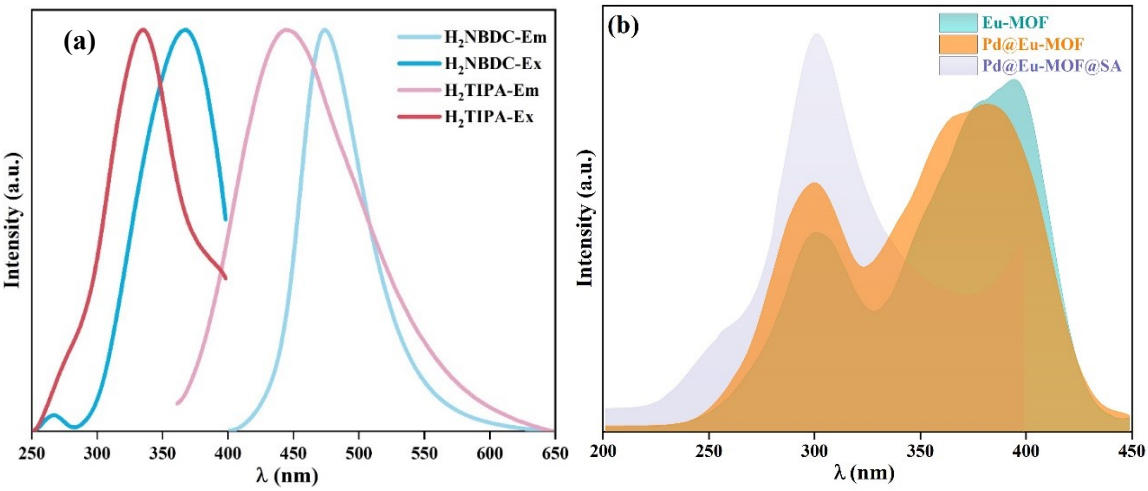

Figure S6. (a) The liquid-emission and excitation spectra of H_2NBDC and H_2TIPA recorded at room temperature; (b) the excitation spectra of Eu-MOF, Pd@Eu-MOF and Pd@Eu-MOF@SA recorded at room temperature.

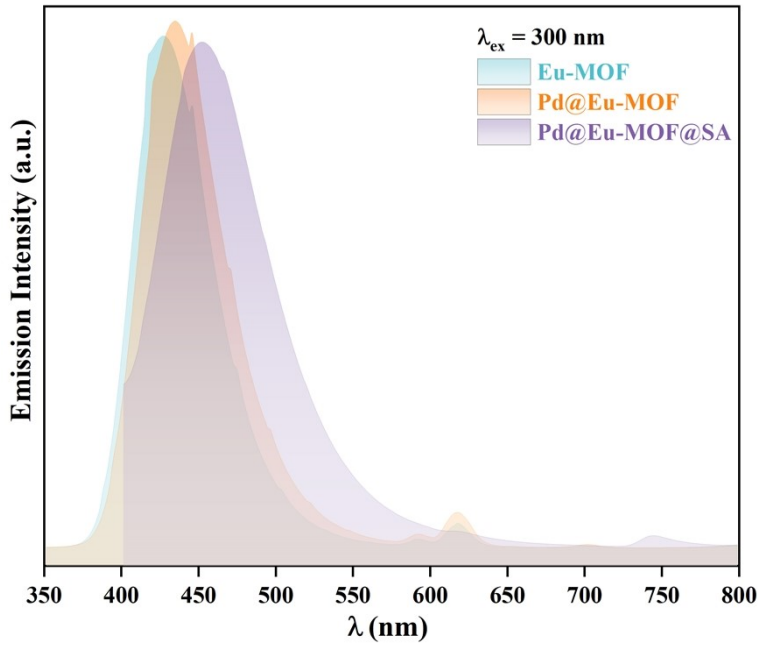

Figure S7. The liquid-emission spectra of Eu-MOF, Pd@Eu-MOF, and Pd@Eu-MOF@SA suspensions recorded at room temperature.

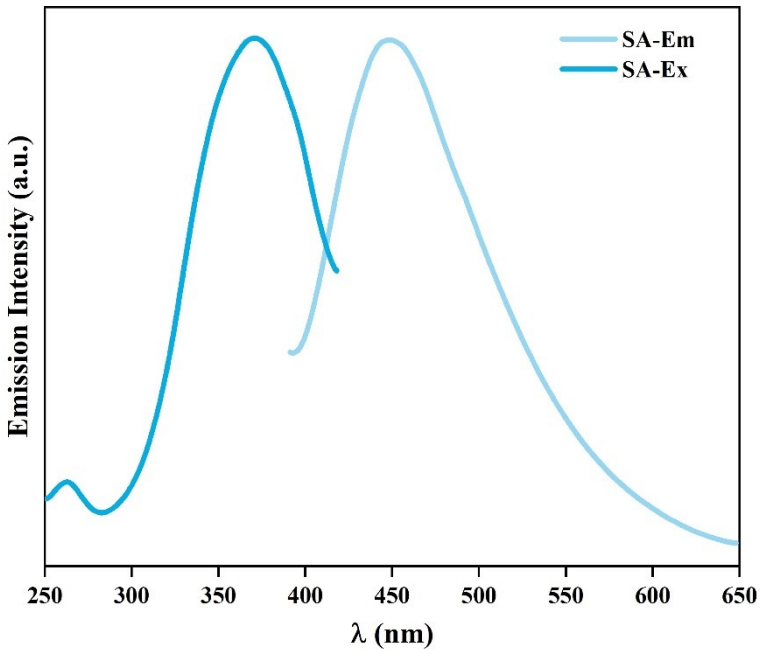

Figure S8. The emission and excitation spectra of the SA gel recorded at room temperature.

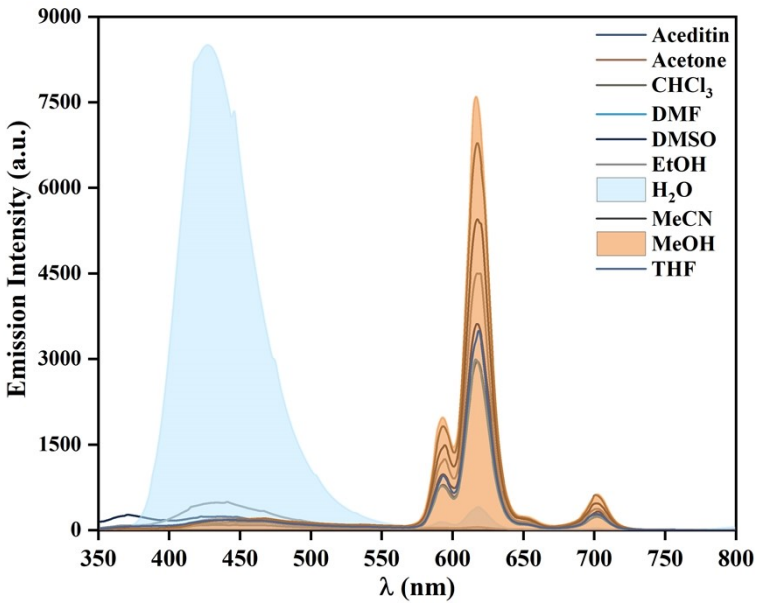

Figure S9. Emission spectra of Eu-MOF in water and nine kinds of organic solvents.

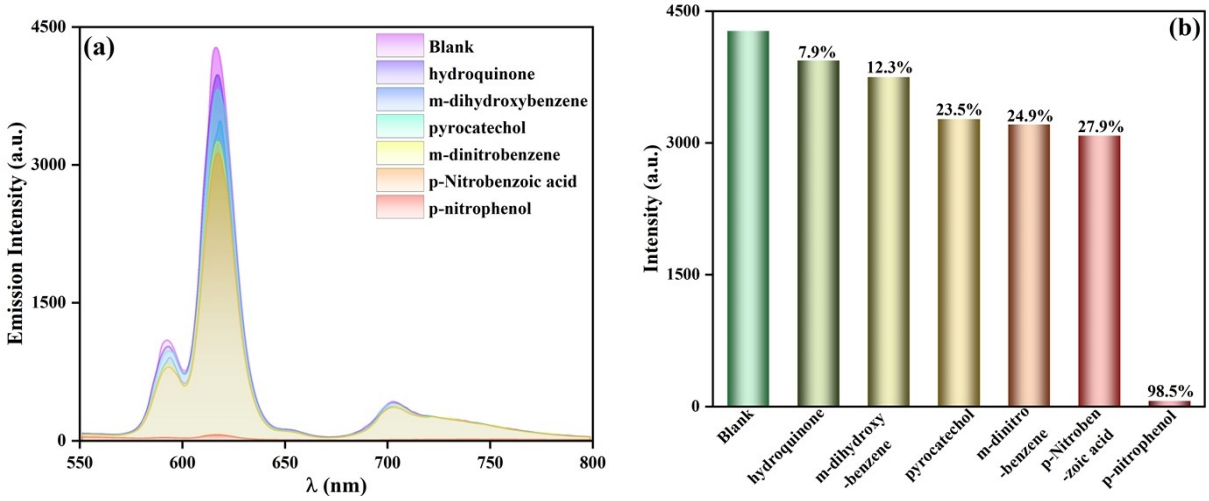

Figure S10. The emission spectra (a) and the comparison in I_{618} (b) of blank Eu-MOF and Eu-MOF sensing hydroquinone, m-dihydroxybenzene, pyrocatechol, m-dinitrobenzene, p-nitrobenzoic acid, and p-NP.

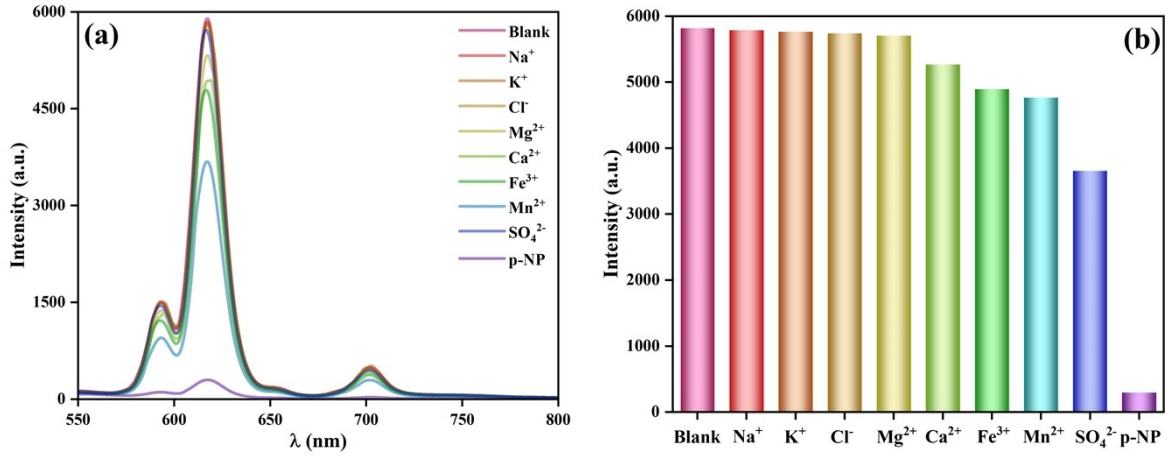

Figure S11. (a) The emission spectra (a) and the comparison in I_{618} of blank Eu-MOF and Eu-MOF with p-Np and the interferents.

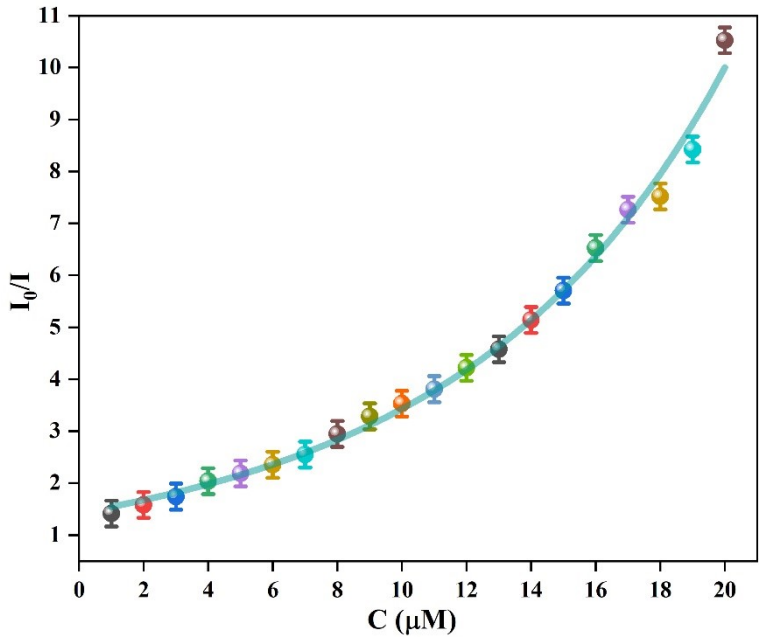

Figure S12. The plot of I_0/I vs $C_{p\text{-}NP}$ and the fitting curve with $C_{p\text{-}NP}$ = 1-20 μM.

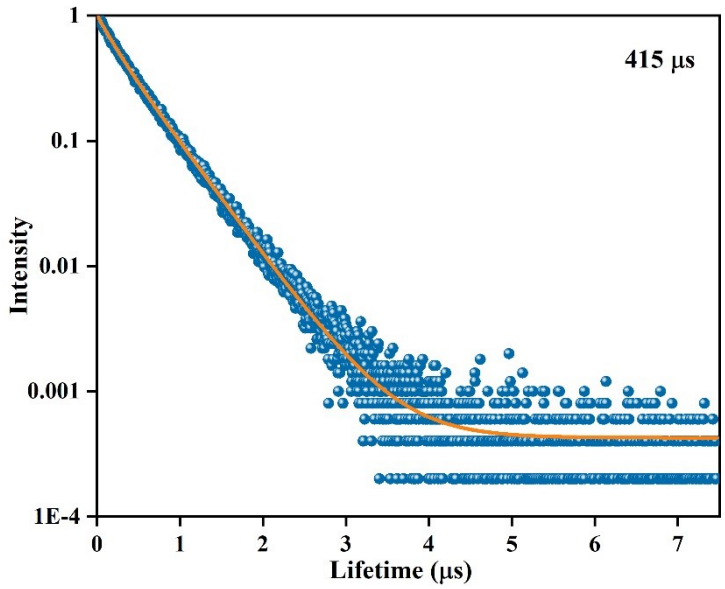

Figure S13. Fluorescence lifetime of Eu^{3+} in blank Eu-MOF.

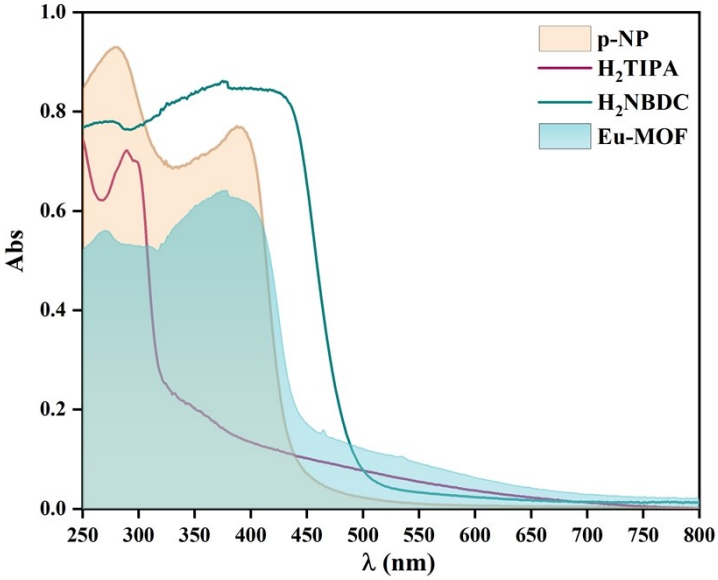

Figure S14. UV-vis spectra of Eu-MOF, p-NP, free H_2TIPA and H_2NBDC ligands.

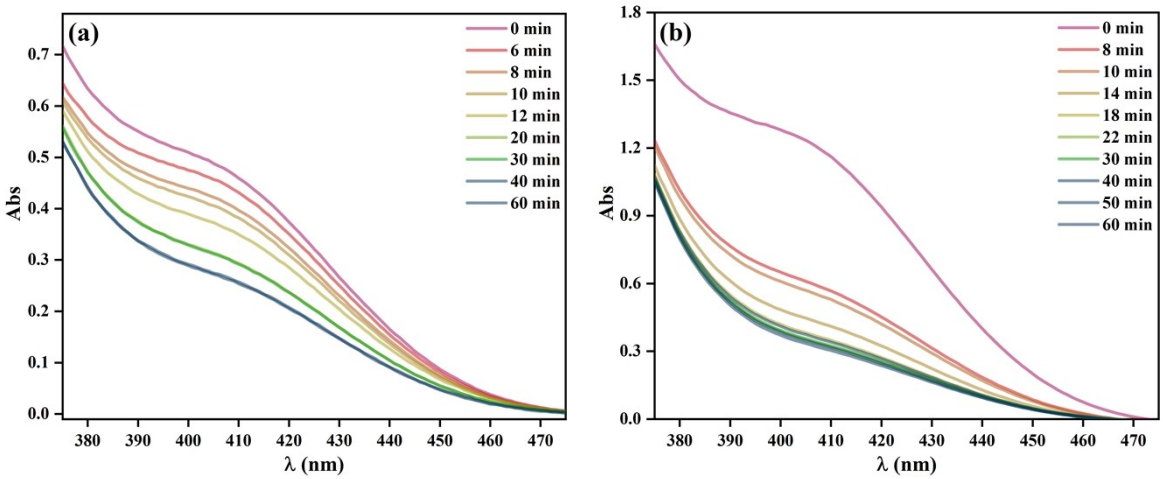

Figure 15. UV-vis spectra of the filtrates after Eu-MOF (a) and Pd@Eu-MOF@SA (b) adsorbing p-NP for 0-60 min.

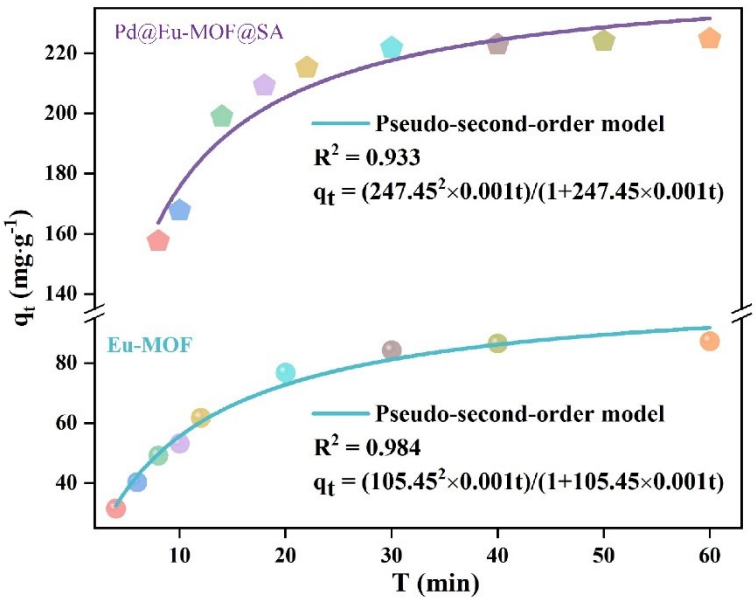

Figure S16. The adsorption kinetics curves of q_t (mg·g^{-1}) *vs* adsorption time (T) for Eu-MOF and Pd@Eu-MOF@SA adsorbing p-NP by the pseudo-second-order model.

Table S3. q_e and the rate constants (k_1 and k_2) of Eu-MOF and Pd@Eu-MOF@SA adsorbing p-NP by the pseudo-first-order and the pseudo-second-order models

Adsorbents	Kinetic model	q_e (mg·g^{-1})	Rate constant	R^2
Eu-MOF	pseudo-first-order	87.83	k_1 = 0.10	0.996
	pseudo-second-order	105.45	k_2 = 0.001	0.984
Pd@Eu-MOF@SA	pseudo-first-order	224.51	k_1 = 0.15	0.991
	pseudo-second-order	247.45	k_2 = 0.001	0.933

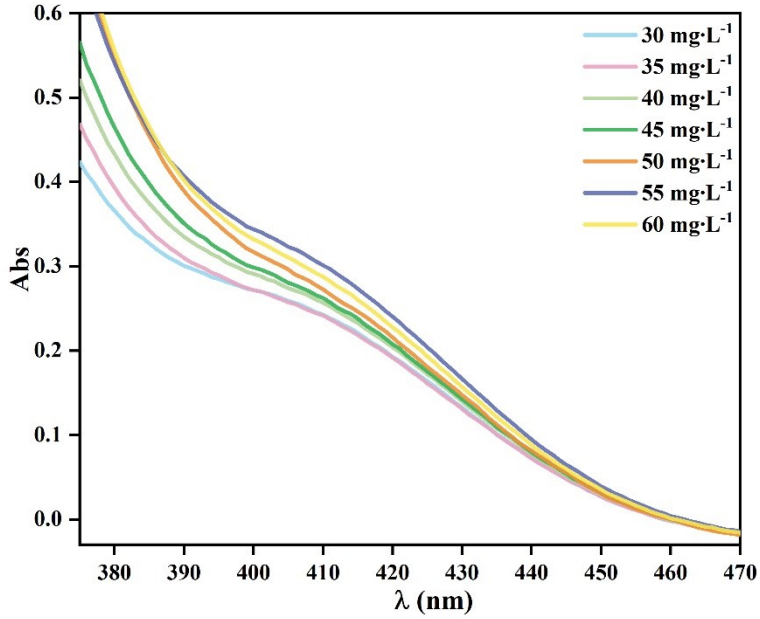

Figure S17. The UV-vis spectra of Eu-MOF adsorbing p-NP with $C_{p\text{-}NP}$ ranging 30-60 mg·L^{-1}.

Table S4. q_{max} and the constants of Freundlich (K_F) and Langmuir (K_L) models for Eu-MOF adsorbing p-NP.

Freundlich model			Langmuir model		
n	K_F ($mg^{-1/n}\cdot L^{1/n}\cdot g^{-1}$)	R^2	q_{max} ($mg\cdot g^{-1}$)	K_L ($L\cdot mg^{-1}$)	R^2
1.26	0.807	0.994	2.62×10^5	8.29×10^{-6}	0.958

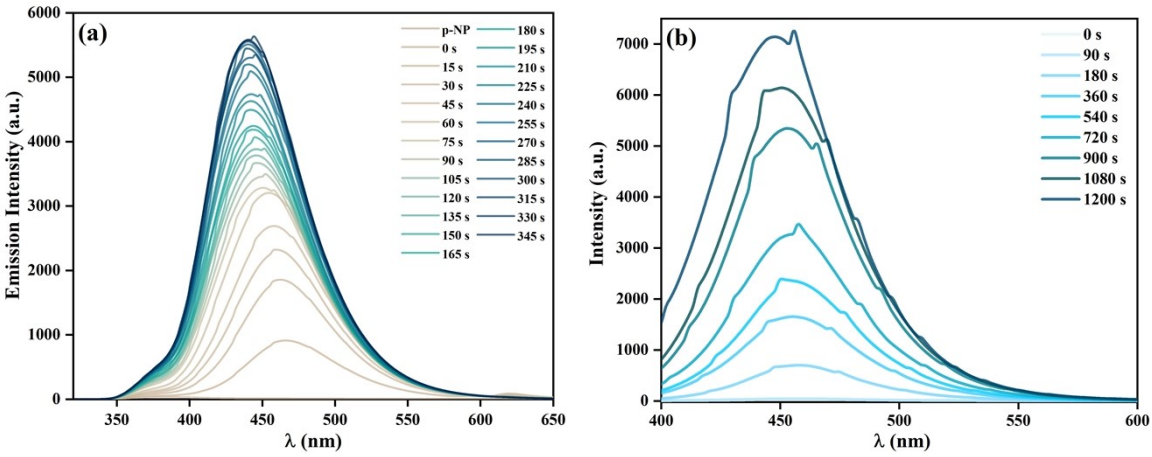

Figure S18. The time-depending emission spectra of Pd@Eu-MOF (a) and Pd@Eu-MOF@SA (b).

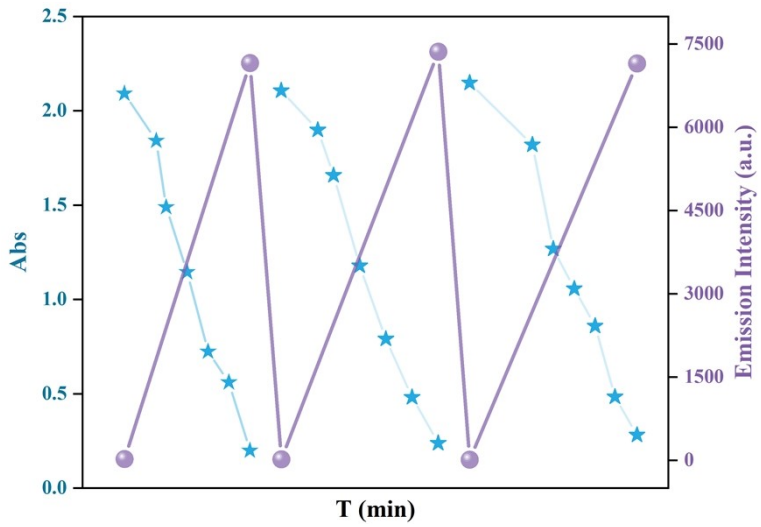

Figure S19. The absorbances of the filtrate and I_{450} of Pd@Eu-MOF@SA in three cycles.

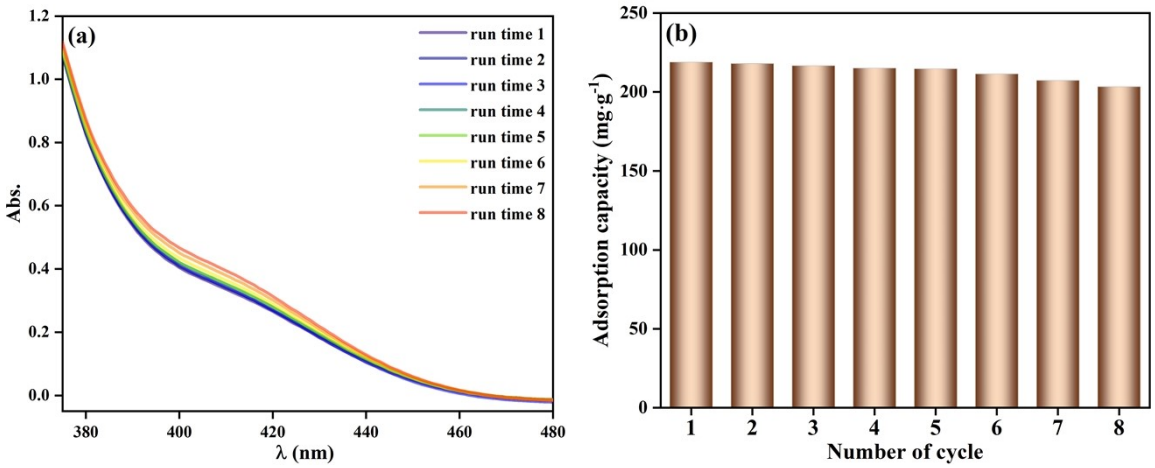

Figure S20. (a) UV-vis spectra of Pd@Eu-MOF@SA adsorbing p-NP in eight adsorption-desorption cycles; (b) the comparison of the adsorption capability in the eight adsorption-desorption cycles.